Investigations into the Membrane Interactions of m-Calpain Domain V

Sarah R. Dennison,* Silvia Dante,† Thomas Hauß,† Klaus Brandenburg,‡ Frederick Harris,* and David A. Phoenix§

*Department of Forensic and Investigative Science, University of Central Lancashire, Preston, United Kingdom; †Berlin Neutron Scattering Centre, Hahn-Meitner-Institut, Berlin, Germany; ‡Division of Biophysics, Forschunginstitut, Borstel, Germany; and §Dean's Office, Faculty of Science, University of Central Lancashire, Preston, United Kingdom

ABSTRACT m-Calpain is a calcium-dependent heterodimeric protease implicated in a number of pathological conditions. The activation of m-calpain appears to be modulated by membrane interaction, which has been predicted to involve oblique-orientated α-helix formation by a GTAMRILGGVI segment located in domain V of the protein's small subunit. Here, we have investigated this prediction. Fourier transform infrared conformational analysis showed that VP1, a peptide homolog of this segment, exhibited α-helicity of ~45% in the presence of dimyristoylphosphatidylcholine/dimyristoylphosphatidylserine (DMPS) vesicles. The level of helicity was unaffected over a 1- to 8-mM concentration range and did not alter when the anionic lipid composition of these vesicles was varied between 1% and 10% DMPS. Similar levels of α-helicity were observed in trifluoroethanol and the peptide appeared to adopt α-helical structure at an air/water interface with a molecular area of 164 $Å^2$ at the monolayer collapse pressure. VP1 was found to penetrate dimyristoylphosphatidylcholine/DMPS monolayers, and at an initial surface pressure of 30 mN m^{-1}, the peptide induced surface pressure changes in these monolayers that correlated strongly with their anionic lipid content (maximal at 4 mN m^{-1} in the presence of 10% DMPS). Neutron diffraction studies showed VP1 to be localized at the hydrophobic core of model palmitoyloleylphosphatidylcholine/palmitoyloleylphosphatidylserine (10:1 molar ratio) bilayer structures and, in combination, these results are consistent with the oblique membrane penetration predicted for the peptide. It would also appear that although not needed for structural stabilization anionic lipid was required for membrane penetration.

INTRODUCTION

Calpains (EC 3.4.22.17) are a superfamily of Ca^{2+}-dependent intracellular cysteine proteases that are ubiquitously distributed in mammalian cells (Perrin and Huttenlocher, 2002; Sorimachi and Suzuki, 2001). Despite intensive study, the physiological functions of these enzymes are not wholly clear but they are believed to play important roles in an array of processes, including: embryonic development, cytoskeletal remodeling, cell differentiation, apoptosis, and signal transduction (Carafoli and Molinari, 1998; Ono et al., 1998; Sato and Kawashima, 2001). Calpains are of medical importance, having been implicated in a range of pathological conditions as diverse as cataract formation, type 2 diabetes, muscular dystrophy, rheumatoid arthritis, ischemic tissue damage/reperfusion, and neurodegenerative conditions (Huang and Wang 2001; Branca 2004). These disorders show a common characteristic of altered Ca^{2+} homeostasis, and it has been suggested that the resulting deregulated activation of calpains may play a role in their development (Perrin and Huttenlocher, 2002).

The most studied member of the calpain superfamily is m-calpain (calpain 2). This enzyme is heterodimeric and, upon activation, undergoes autolytic conversion to give its mature proteolytic form. The larger subunit of m-calpain is 80 kDa and organized into four domains (I–IV). Domain II houses the enzyme's active site, which is a papainlike cysteine protease domain (Tompa, 2001), whereas domain I forms an N-terminal extension of domain II and is associated with m-calpain autolysis. Domain III appears to be a linker region between the catalytic domain and domain IV, which contains a calmodulinlike Ca^{2+}-binding domain with multiple EF-hands. The smaller subunit of m-calpain is 30 kDa and possesses two domains (V and VI). Domain VI possesses a calmodulinlike Ca^{2+} binding domain and associates with domain IV to facilitate dimerization of the m-calpain subunits, whereas domain V is largely cleaved from m-calpain during autolysis (Goll et al., 2003).

It is well established that for in vitro activation m-calpain requires millimolar levels of Ca^{2+} that are far in excess of those found in vivo, clearly suggesting that activation of the enzyme involves other factors (Johnson and Guttmann, 1997; Hosfield et al., 2004). A membrane-associated form of m-calpain is known and a number of studies have shown that the presence of lipid can strongly reduce the Ca^{2+} concentrations required for activation of the enzyme (Imajoh et al., 1986; Melloni and Pontremoli, 1989; Saido et al., 1992) to within range of those found in physiological systems (Chakrabarti et al., 1996). These results have led to the suggestion that lipid/membrane interactions could play a role in the activation of m-calpain (Johnson and Guttmann, 1997), and based on in vitro studies, two regions of the enzyme have been separately proposed to facilitate such interactions.

Submitted July 16, 2004, and accepted for publication January 11, 2005.

Address reprint requests to D. A. Phoenix, Dean's Office, Faculty of Science, University of Central Lancashire, Preston PR1 2HE, UK. Tel.: 1772-893481; Fax: 1772-894981; E-mail: daphoenix@uclan.ac.uk.

0006-3495/05/04/3008/10 $2.00

doi: 10.1529/biophysj.104.049957

Recent studies have shown that domain III of m-calpain binds lipid in a Ca^{2+} dependent manner (Tompa, 2001) and forms an antiparallel β-sheet structure that possesses distant structural resemblances to C2 domains (Hosfield et al., 1999, 2004; Strobl et al., 2000). Such domains are believed to modulate enzyme activity via Ca^{2+}-regulated lipid binding (Rizo and Sudhof, 1998; Verdaguer et al., 1999) and it has been proposed that a similar mechanism may allow domain III to modulate the activation of m-calpain (Reverter et al., 2001).

Previous studies have suggested that interactions between domain V of m-calpain and lipid are able to lower the enzyme's Ca^{2+} requirement for activation (Arthur and Crawford, 1996; Crawford et al., 1990). More recently, theoretical analyses of domain V from a number of mammalian m-calpains identified a common sequence, GTAMRILGGVI, with the potential to form a lipid interactive α-helix. This was confirmed by experimental results and further theoretical analysis predicted that the α-helix possessed structural amphiphilicity and a gradient in hydrophobicity similar to those of known oblique-orientated α-helices (Brandenburg et al., 2002). Based on these structural similarities, it was proposed that the GTAMRILGGVI α-helix might utilize a similar mechanism of membrane interaction, penetrating the membrane hydrophobic core region in an oblique orientation (Daman et al., 2001).

Here, we have investigated this prediction and studied the ability of VP1, a peptide homolog of the GTAMRILGGVI segment, to penetrate lipid assemblies, mimetic of naturally occurring membranes. Fourier transform infrared spectroscopy (FTIR) conformational analysis and lipid monolayer studies showed that VP1 strongly penetrates phosphatidylcholine/phosphatidylserine monolayers via α-helix formation. Moreover, neutron diffraction showed that VP1 localizes at the hydrophobic core region of model bilayers with a similar lipid composition. We discuss our results in relation to the oblique form of membrane penetration predicted for the GTAMRILGGVI segment of m-calpain.

MATERIALS AND METHODS

Reagents

The peptide VP1 was supplied by Albachem (Gladsmuir, UK), synthesized by solid-state synthesis and purified by high-performance liquid chromatography to purity >99%, confirmed by matrix-assisted laser desorption/ionization mass spectrometry. Buffers and solutions for monolayer experiments were prepared from Milli-Q water. Palmitoyloleylphosphatidylcholine (POPC) and palmitoyloleylphosphatidylserine (POPS) were purchased from Avanti Polar Lipids (Alabaster, AL). Dioleoylphosphatidylcholine (DOPC), dioleoylphosphatidylserine (DOPS), dimyristoylphosphatidylcholine (DMPC), and dimyristoylphosphatidylserine (DMPS) were purchased from Alexis (Bingham, UK). All other reagents were purchased from Sigma (Bracknell, UK).

Monolayer studies

Langmuir-Blodgett studies

Monolayer studies were conducted at a constant temperature of 21.0 ± 1°C using Langmuir-Blodgett equipment supplied by NIMA technology (Canley, UK). Studies were conducted using a Teflon trough with surface area dimensions of 5 × 15 cm and holding a volume of 80 ml. The trough was equipped with moveable barriers, the position of which could be adjusted at a rate of 6 cm^2 min^{-1}. For all experiments, a buffer subphase of 10 mM Tris buffer, pH 7.5, was utilized and, unless indicated otherwise, VP1 was introduced into the subphase via an injection port to give desired final concentrations. The subphase was continuously stirred by a magnetic bar (5 rpm) and surface tension was monitored by the Wilhelmy method using a paper plate (Whatman's Ch1) in conjunction with a microbalance, as described by Brandenburg et al. (2002). Changes in monolayer surface pressure/area were recorded as graphic output on a PC using NIMA software, which interfaces with the Langmuir-Blodgett microbalance.

VP1 surface activity

The barriers of the Langmuir-Blodgett trough were adjusted to their maximum separation (surface area 86 cm^2) and this position was maintained. VP1 was then introduced into the buffer subphase to give final concentrations ranging between 1.0 and 25.0 μM, and at each peptide concentration changes in surface pressure at the air/water interface were monitored. The maximal values of these surface pressure changes were then plotted as a function of VP1 final subphase concentration (Fig. 1). From these results the surface excess, Γ, was calculated by means of the Gibbs adsorption isotherm, which is given by Eq. 1 (Birdi, 1999):

$$\Gamma = -\frac{1}{RT}\frac{\Delta\pi}{\Delta \ln c}, \tag{1}$$

where R is 8.314 J mol^{-1} K^{-1}, $T = 294$ °K, π is the interfacial pressure increase (mN m^{-1}), and c is the molar concentration of peptide in the subphase (M). These values of Γ were then used to determine values of the interfacial surface area per VP1 molecule (A) according to the equation

$$A = \frac{1}{N\Gamma}, \tag{2}$$

where N is Avogadro's number (Table 1).

In addition, the ability of VP1 to spread on an aqueous surface and to form a stable monolayer was investigated. The barriers of the Langmuir-Blodgett trough were adjusted to their maximum separation (surface area 86 cm^2) and this position was maintained. A 10-μl aliquot of VP1 in chloroform (0.8 mM) was spread onto a buffer subphase and allowed to equilibrate for 1 h. The resulting peptide monolayer was compressed using

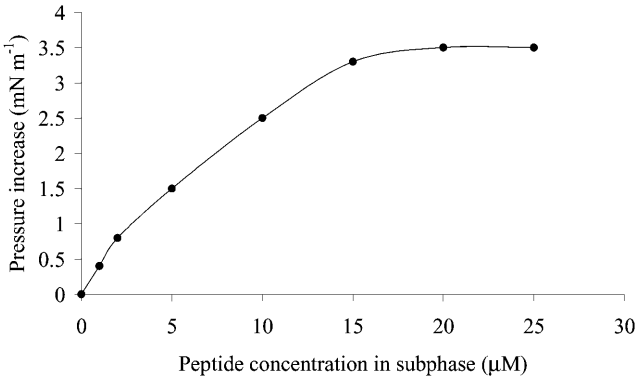

FIGURE 1 Surface activity of VP1 showing the effect of VP1 concentration on the surface pressure of an air/water interface. Varying concentrations of VP1 were injected into the subphase (10 mM Tris, pH 7.5) of a Langmuir-Blodgett system and allowed to equilibrate for 30 min. For each VP1 concentration, the surface pressure of the subphase was then determined and these values plotted.

TABLE 1 The surface excess and area/molecule for different VP1 peptide concentrations

C (μM)	π (mN m^{-1})	Γ	Area (Å^2)
1	0.4	2.37×10^{-8}	7005.49
2	0.8	5.27×10^{-8}	3150.48
5	1.5	1.16×10^{-7}	1431.29
10	2.5	2.22×10^{-7}	747.77
15	3.3	3.21×10^{-7}	516.62
20	3.5	3.66×10^{-7}	453.63
25	3.5	3.88×10^{-7}	427.91

Γ is the surface excess, C is the molar concentration of the peptide in the subphase, and π is the interfacial pressure increase.

the moveable barriers of the trough to produce a pressure/area isotherm, which was converted by NIMA software to an output plot of surface pressure versus monolayer surface area per VP1 molecule (Fig. 2).

Insertion of VP1 into lipid monolayers at constant area

The ability of VP1 to penetrate lipid monolayers at constant area was studied. Monolayers were formed by spreading lipid mixtures (5 mM) in chloroform of either DMPC/DMPS or DOPC/DOPS (each at a 10:1 molar ratio) onto a buffer subphase. The solvent was allowed to evaporate off over 30 min and then the monolayer was compressed at a velocity of 6 cm^2 min^{-1} to give a surface pressure of 30 mN m^{-1}. The lipid monolayer was then maintained at the area corresponding to this pressure throughout the experiment. VP1 was introduced into the subphase to give a final peptide concentration of 20 μM and interactions of the peptide with lipid monolayers were monitored as changes in monolayer surface pressure versus time (Fig. 3).

The ability of VP1 to penetrate DMPC/DMPS monolayers at different molar ratios was studied. Chloroform solutions (5 mM) of DMPC/DMPS at molar ratios of either 100:1, 50:1, 20:1, or 10:1 were spread onto a buffer subphase and compressed to a lateral pressure of 30 mN m^{-1}, as described above. The lipid monolayer was then maintained at the area corresponding to this pressure throughout the experiment. VP1 was introduced into the subphase to give a final peptide concentration of 20 μM and maximal changes in monolayer surface pressure were plotted versus the anionic lipid content of the monolayer (Fig. 4).

Interaction of VP1 with lipid monolayers at constant pressure

The ability of VP1 to penetrate lipid monolayers at constant pressure was studied. Chloroform solutions (5 mM) of DMPC/DMPS at molar ratios of either 100:1, 50:1, 20:1, or 10:1 were spread onto a buffer subphase. The solvent was allowed to evaporate off for 30 min and the monolayer compressed at a velocity of 6 cm^2 min^{-1} to give a surface pressure of 30 mN m^{-1}. The lipid monolayer was then maintained at this pressure throughout the experiment. The monolayer was allowed to equilibrate for 10 min and then VP1 was introduced into the subphase to give a final peptide concentration of 20 μM. Interactions of the peptide with lipid monolayers were monitored by NIMA software, which provided an output plot of changes in monolayer surface area per lipid molecule versus time (Fig. 5).

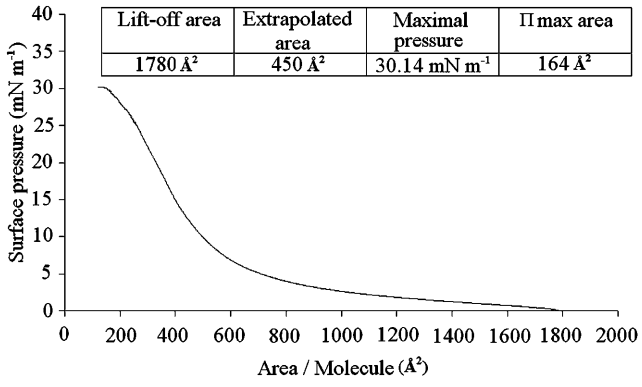

FIGURE 2 Compression isotherm of VP1 showing a pressure-area isotherm for a VP1 monolayer, which was spread from chloroform onto a subphase of 10 mM Tris, pH 7.5.

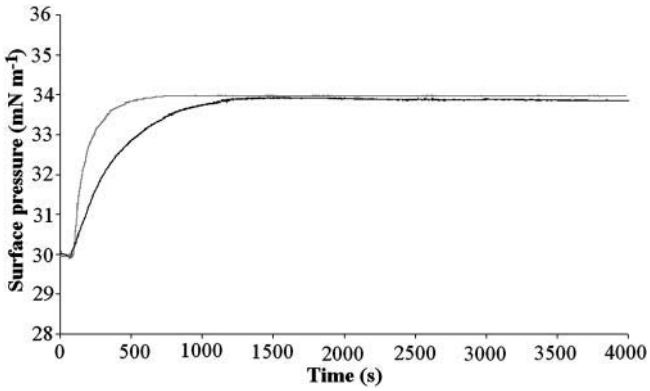

FIGURE 3 Monolayer interactions of VP1 showing the time course of VP1/lipid monolayer interactions. Monolayers of DMPC/DMPS (*upper shaded trace*) and DOPC/DOPS (*black trace*) (10:1 molar ratio) were constructed with an initial surface pressure of 30 mN m^{-1}, mimetic of a naturally occurring membrane. For each case studied, the introduction of VP1 (20 μM) into the subphase led to monolayer interactions that appeared to follow hyperbolic kinetics and maximal surface pressure increases of 4 mN m^{-1}.

FTIR spectroscopy

Sample preparation

Small unilamellar vesicles (SUVs) were prepared according to Keller et al., (1992). Essentially, DMPC/DMPS mixtures in chloroform were prepared, dried with nitrogen, and rehydrated with aqueous *N*-[2-hydroxyethylpiperazine-*N*′-[2-ethanesulphonic acid] (HEPES) at pH 7.5 to give desired final lipid molar ratios. The resulting cloudy suspensions were sonicated at 4°C with a Soniprep (Foster City, CA) 150 sonicator until clear suspensions resulted (30 cycles of 30 s) which were then centrifuged (15 min, 3000 $\times$ g, 4°C).

The effect of varying vesicle lipid composition on levels of VP1 secondary structure was studied. VP1 (final concentration 8 mM) was solubilized in vesicle suspensions prepared as described above, where the overall lipid/VP1 ratio was maintained at 100:1 but the DMPC/DMPS ratio ranged between 10:1 and 100:1 (Fig. 6 *A*, Table 2). The effect of varying the total lipid/peptide ratio on levels of VP1 secondary structure was also studied. VP1 (final concentration 8 mM) was solubilized in vesicle suspensions prepared as described above, where the DMPC/DMPS ratio was maintained at 10:1 but the overall lipid to VP1 ratio was varied between 100:1 and 10:1 (Fig. 6 *B*). Additionally, the effect of final VP1 concentration on levels of secondary structure shown by the peptide in the presence of lipid vesicles was studied. VP1 (final concentration ranging between 8 mM and 1 mM) was solubilized in vesicle suspensions prepared as described above, where the overall lipid to VP1 ratio was maintained at 100:1 and the DMPC/DMPS ratio was maintained at 10:1 (Table 3).

FTIR conformational analyses of VP1 in the presence of lipid

All samples prepared as described above were individually spread on a CaF_2 crystal, and the free excess water evaporated at room temperature. The single

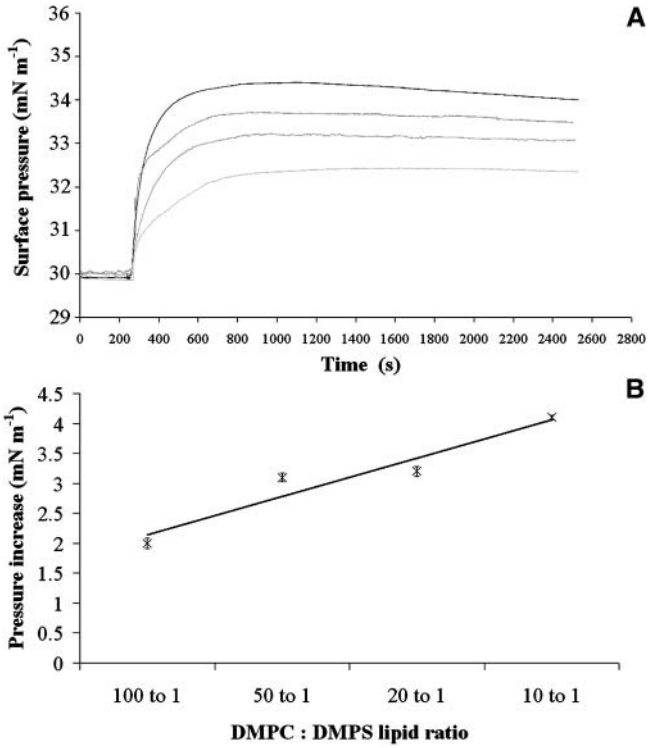

FIGURE 4 Change in surface pressure against different lipid ratios. (*A*) Surface pressure changes at constant area after adding VP1 (20 μM) to the subphase in the presence of 100:1 DMPC/DMPS (*lower trace*), 50:1 DMPC/DMPS (*middle light shaded trace*), 20:1 DMPC/DMPS (*upper dark shaded trace*), and 10:1 DMPC/DMPS (*upper black trace*). (*B*) As the level of anionic lipid in the DMPC/DMPS monolayers is increased, the maximal level of VP1 interaction with the lipid monolayer rises. Error bars represent the standard error on four replicates.

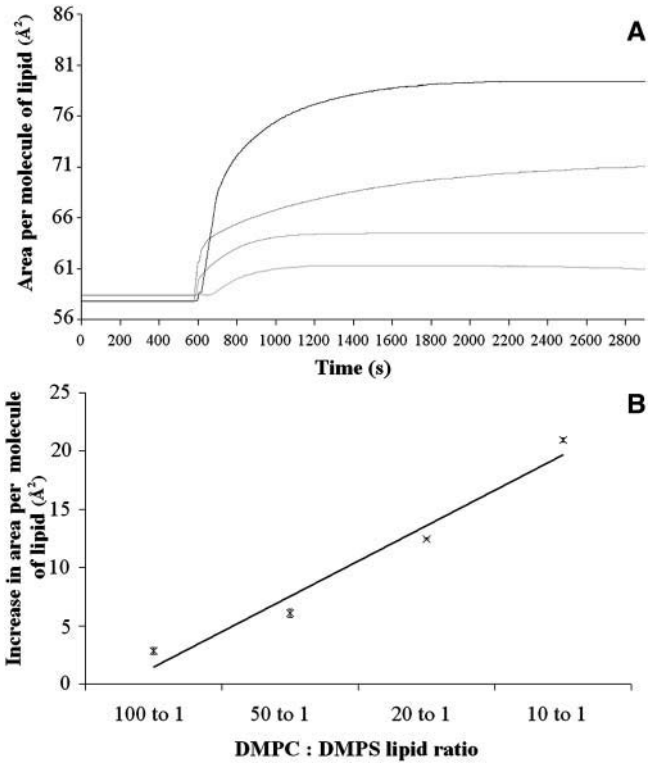

FIGURE 5 Change in area against different lipid ratios. (*A*) Monolayer expansions at constant surface pressure after adding VP1 (20 μM) to the subphase in the presence of 100:1 DMPC/DMPS (*lower trace*), 50:1 DMPC/DMPS (*middle light shaded trace*), 20:1 DMPC/DMPS (*upper dark shaded trace*), and 10:1 DMPC/DMPS (*upper black trace*). (*B*) Summary of the relationship between lipid ratio and area per lipid molecule. Error bars represent the standard error on four replicates.

band components of the VP1 amide I vibrational band (predominantly C=O stretch) was monitored using an FTIR 5DX spectrometer (Nicolet Instruments, Madison, WI) and absorbance spectra were produced for each sample. For these spectra, water bands were subtracted and the evaluation of peptide band parameters (peak position, band width, and intensity) was performed. Curve fitting was applied to overlapping bands using a modified version of the CURFIT procedure written by D. Moffat (National Research Council, Ottawa, Canada). The band shapes of the single components are superpositions of Gaussian and Lorentzian band shapes. Best fits were obtained by assuming a Gauss fraction of 0.55–0.6. The CURFIT procedure measures the peak areas of single-band components and, after statistical evaluation, determines the relative percentages of primary structure involved in secondary structure formation.

Neutron diffraction studies

Neutron diffraction experiments were conducted using the V1 membrane diffractometer at BENSC and analytical techniques previously described (Bradshaw et al., 1997, 1998, 2000; Duff et al., 1994; Hauβ et al., 2002). Essentially: solutions of POPC/POPS (10:1 molar ratio) in chloroform were prepared. Aliquots (1 ml) of these lipid solutions, and these solutions containing VP1 (8 mM), were evenly deposited onto separate quartz microscope slides using an artist's airbrush (Aerobrush pro281, Hansa, Norderstedt, Germany). These treated slides were placed in a vacuum desiccator for 12 h to remove all traces of chloroform. Each slide was then individually placed in an aluminium thermostat sample can and rehydrated for 24 h at 25°C with relative humidity maintained at 98% using Teflon water baths containing saturated potassium sulfate solution. Potassium sulfate water solutions at each of three isotopic compositions, 50%, 20%, and 8% ^2H_2O, were used to assist with phase assignment. Under these conditions, lipid samples self-assemble to form multilamellar structures that may be considered as stacked membrane bilayers. After each completed neutron diffraction measurement, a given quartz sample slide was rehydrated with water at the next isotopic composition, with at least 24 h allowed for equilibration. The scanning procedure consisted of sequential θ scans around the predicted Bragg angle for each order. The rocking scans covered the Bragg position θ for the angle $\theta \pm 2°$. Diffraction patterns of the prepared samples were measured with up to five orders detected for each sample.

The raw data from the two dimensional detector were summed to intensity versus 2θ using the V1 instrumental software. The commercial software IGOR Pro (version 4) was used for all further data treatment. The lamella (bilayer) spacing d for each sample, was calculated by least-square fitting of the observed 2θ values to the Bragg equation:

$$N\lambda = 2d \sin\theta, \tag{3}$$

where n is the diffraction order and λ is the neutron wavelength (4.52 Å).

The integrated intensities were calculated based upon the Gaussian fit of the experimental Bragg reflections. Absorption correction and Lorentz factor were applied and their intensities square-rooted to produce structure-factor amplitudes. The phase assignment of each order and the relative scaling of the different datasets were determined by least-squares fitting to straight-line functions (Dante et al., 2002). The scattering length density profiles $\rho(z)$ were then calculated for each sample using the formula

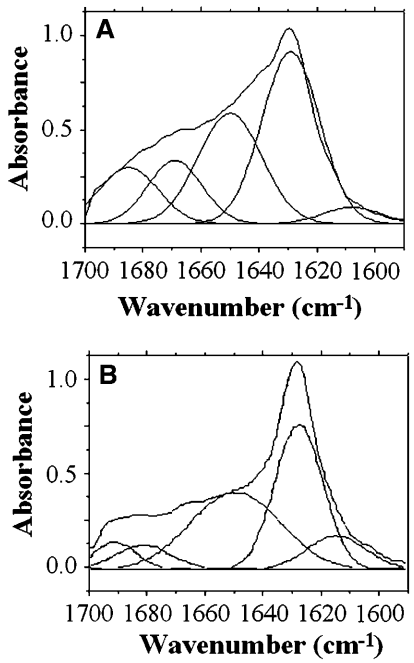

FIGURE 6 Conformational analysis of VP1 in the presence of lipid. (*A*) A spectrum representing FTIR conformational analyses of VP1 (8 mM) in the presence of DMPC/DMPS (10:1 molar ratio) vesicles at a total lipid/peptide molar ratio of 100:1. (*B*) A spectrum of a corresponding system except that the total lipid/peptide molar ratio is 10:1. It can be seen that in both cases there is a major band at 1649 cm^{-1} showing that the peptide possesses high levels of α-helical structure (45% and 48%, respectively).

$$\rho(z) = \rho_0 + 2/d\Sigma f(h)\cos((2\pi hz)/d, \quad (4)$$

where $\rho_0(z)$ is the integral density per unit length of the bilayer, f(h) are the scaled structural factors, and the second term describes the distribution in the scattering lengths across the bilayer.

RESULTS

Monolayer studies

VP1 surface activity

VP1 was introduced into the buffer subphase of the Langmuir-Blodgett trough to give a range of final peptide concentrations. In each case, changes in the interfacial surface pressure were monitored and maximal values of these pressure changes were plotted against the corresponding final peptide concentrations (Fig. 1). It can be seen from Fig. 1 that these pressure changes increase in an approximately linear manner with rising VP1 concentration until at 20 μM peptide, the maximal value is observed. Above this peptide concentration, surface pressures are effectively constant. Thus 20 μM VP1 was the minimum bulk concentration required to saturate the air/water interface with the peptide under these experimental conditions and was used as the VP1 subphase concentration in all subsequent monolayer studies. Additionally, these data were used to determine the corresponding interfacial surface area per VP1 molecule (Table 1) and for 20 μM peptide this can expand to 453 $Å^2$ which is comparable to that found for other α-helical peptides (Ambroggio et al., 2004).

TABLE 2 The levels of secondary structure exhibited by VP1 in the presence of vesicles formed form DMPC/DMPS when the anionic content of these vesicles was varied

Overall lipid/VP1 ratio	DMPC/DMPS ratio	Levels of secondary structure in VP1 (8 mM)	
		α-helix	β-sheet
100:1	10:1	44	26
100:1	25:1	43	27
100:1	50:1	46	23
100:1	100:1	47	26

TABLE 3 The effect of varying VP1 concentration on the levels of secondary structure exhibited by the peptide in the presence of vesicles formed from DMPC/DMPS

Overall lipid/VP1 ratio	DMPC/DMPS ratio	VP1 (mM)	Levels of VP1 secondary structure	
			α-helix	β-sheet
100:1	10:1	8	41	25
100:1	10:1	4	46	22
100:1	10:1	2	43	23
100:1	10:1	1	45	25

The ability of VP1 to spread on an aqueous surface and to form a stable monolayer was investigated. VP1 in chloroform was spread on to a buffer subphase and a plot of surface pressure versus monolayer surface area per VP1 molecule generated (Fig. 2). Fig. 2 shows that the collapse pressure of the isotherm starts around 30 mN m^{-1}, indicating the presence of a well-ordered monolayer (Alminana et al., 2003). Fig. 2 also shows that the area per VP1 molecule corresponding to this collapse pressure was 164 $Å^2$, which is consistent with the presence of α-helical structure in VP1 (Fidelio et al., 1986). The extrapolated area at n = 0 mN m^{-1} for the isotherm provides a measure of the mean monolayer surface area per VP1 molecule (Sospedra et al., 1999). This area was 450 $Å^2$ per VP1 molecule and is comparable to the value of 453 $Å^2$ calculated above using Eqs. 1 and 2 (Table 1).

Insertion of VP1 into lipid monolayers at constant area

The ability of VP1 to penetrate lipid monolayers at constant area was studied. Monolayers of either: DMPC/DMPS or DOPC/DOPS (each at a 10:1 molar ratio) were spread onto a buffer subphase and compressed to give an initial surface pressure of 30 mN m^{-1}. With constant monolayer area maintained, VP1 was introduced into the subphase to give a final peptide concentration of 20 μM and interactions of the peptide with lipid monolayers were monitored as changes in

monolayer surface pressure versus time (Fig. 3). It can be seen from Fig. 3 that for each of the monolayers studied, the insertion of VP1 followed hyperbolic kinetics. In each case, the final surface pressure change induced by VP1 was ~4 mN m^{-1} although the time taken to induce these changes showed significant variation (300 s and 1500 s, respectively).

The ability of VP1 to penetrate DMPC/DMPS monolayers at different molar ratios was studied. Monolayers of DMPC/DMPS at molar ratios of either 100:1, 50:1, 20:1, or 10:1 were spread onto a buffer subphase and compressed to an initial surface pressure of 30 mN m^{-1}. With constant monolayer area maintained, VP1 was introduced into the subphase to give a final peptide concentration of 20 μM and monolayer surface pressure was plotted versus time (Fig. 4 *A*). Fig. 4 *A* shows that in each case VP1 induced an increase in surface pressure, which followed a hyperbolic time course. Maximal changes in monolayer surface pressure were then plotted against the anionic lipid content of the monolayer (Fig. 4 *B*). The regression analysis in Fig. 4 *B* indicates a strong correlation between these parameters ($R^2 = 0.97$). As the level of anionic lipid in the DMPC/DMPS monolayer is increased, the maximal level of VP1 interaction with the lipid monolayer rises.

Interaction of VP1 with lipid monolayers at constant pressure

The ability of VP1 to penetrate lipid monolayers at constant pressure was studied. Monolayers of DMPC/DMPS at molar ratios of either 100:1, 50:1, 20:1, or 10:1 were spread onto a buffer subphase and compressed to give a surface pressure of 30 mN m^{-1}, giving rise to an area of 58.4 $Å^2$ per molecule of pure lipid. With constant pressure maintained, VP1 was introduced into the subphase and output indicating changes in monolayer surface area per lipid molecule versus time was monitored (Fig. 5 *A*). Fig. 5 *A* shows that in each case VP1 induced significant expansion of monolayers, which followed a hyperbolic time course but with differing kinetics. Fig. 5 *A* shows that the maximum increase in monolayer surface area per molecule of lipid was 79.4 $Å^2$ for DMPC/DMPS at a molar ratio of 10:1. The level of these area changes decreased with decreasing anionic content of monolayers until, in the presence of DMPC/DMPS at a molar ratio of 100:1, the monolayer expanded to 61.2 $Å^2$ per molecule of lipid, representing a 22% decrease in area compared to the 10:1 lipid ratio. The regression analysis in Fig. 5 *B* shows a strong correlation ($R^2 = 0.96$) between these parameters. Here the area decrease is inversely proportional to the anionic content of the monolayer.

FTIR spectroscopy

The effect of varying lipid vesicle composition on levels of VP1 secondary structure was studied. VP1 (final concentration 8 mM) was solubilized in vesicle suspensions where the overall lipid/VP1 ratio was maintained at 100:1 but the DMPC/DMPS ratio was varied between 10:1 and 100:1. Levels of VP1 α-helicity and β-sheet structure were then determined (Fig. 6 *A* and Table 2). Table 2 shows that decreasing the level of DMPS in these vesicles from 10% to 1% led to no significant variation in levels of VP1 α-helicity or β-sheet structure, which were ~45% and 25%, respectively.

The effect of varying the total lipid/peptide ratio on levels of VP1 secondary structure was also studied. VP1 (final concentration 8 mM) was solubilized in vesicle suspensions where the DMPC/DMPS ratio was maintained at 10:1 but the overall lipid/VP1 ratio was varied between 10:1 and 100:1. Levels of VP1 α-helicity were then determined and were found to be 48% in the presence of vesicle suspensions at a 10:1 total lipid/peptide ratio (Fig. 6 *B*) and 45% in the presence of vesicle suspensions at a 100:1 total lipid/peptide ratio (Fig. 6 *A*).

The effect of final VP1 concentration on levels of secondary structure shown by the peptide in the presence of lipid vesicles was studied. VP1 (final concentration ranging between 8 mM and 1 mM) was solubilized in vesicles where the overall lipid/VP1 ratio was maintained at 100:1 and the DMPC/DMPS ratio was maintained at 10:1. Levels of VP1 α-helicity and β-sheet structure were then determined (Table 3). Table 3 shows that between 1 mM and 8 mM of VP1, no significant variations in levels of either α-helicity or β-sheet structure (~45% and 25%, respectively) were observed.

Neutron diffraction studies

The interactions of VP1 with POPC/POPS bilayers was studied. The *d*-spacings obtained in the absence and presence of peptide were 55.0 ± 0.2 Å indicating that the membrane thickness and hydration were not affected by the peptide. The structure factors from Table 4 were used to determine the neutron diffraction density profiles using an 8% ^2H_2O contrast. At this $H_2O/^2H_2O$ ratio, the mean neutron scattering length of the water mixture is zero (King and White, 1986). Fig. 7 *A* shows the neutron scattering density profile of a transection taken perpendicular to the surface of these lipid bilayers in the absence of VP1. The two maxima of the profile indicate that the highest levels of neutron scattering occur in the bilayer lipid headgroup regions (King and White, 1986). The minimal peaks are associated with double bonds on the

TABLE 4 Experimental structure factors *F*(*h*), corrected and scaled as described in the text

	F(1)	*F*(2)	*F*(3)	*F*(4)	*F*(5)
POPC/POPS	0.634 ± 0.002	−0.595 ± 0.002	−0.045 ± 0.003	−0.100 ± 0.008	0.171 ± 0.004
POPC/POPS + VP1	0.584 ± 0.002	−0.650 ± 0.002	−0.461 ± 0.004	0	0.150 ± 0.003

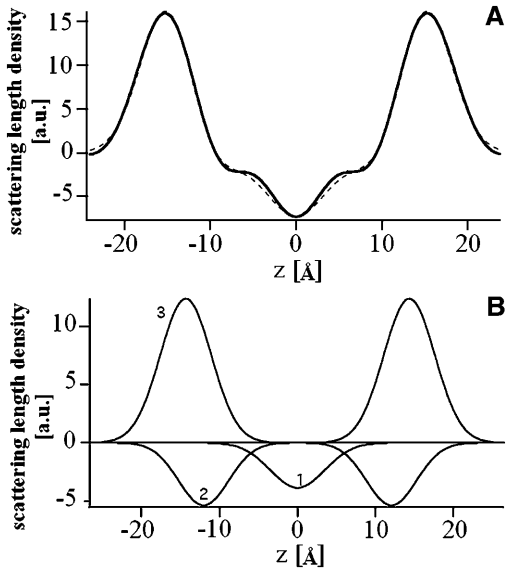

FIGURE 7 Neutron scattering length density profiles of lipid bilayers. (*A*) Neutron scattering density profile generated by a transect of a POPC/POPS (10:1 molar ratio) membrane bilayer taken perpendicular to the bilayer surface (*solid line*). The two maxima of the profile indicate that the highest levels of neutron scattering are shown by the bilayer lipid headgroup regions, whereas the minimum indicates that the lowest levels are generated by lipid terminal methyl groups located at the center of the bilayer hydrophobic core. Each profile was determined at 8% ^2H_2O contrast. (*B*) Superpositions of the various curves representing the different submolecular lipid groups: polar head (*3*); methyl group (*1*), and alkyl chains (*2*).

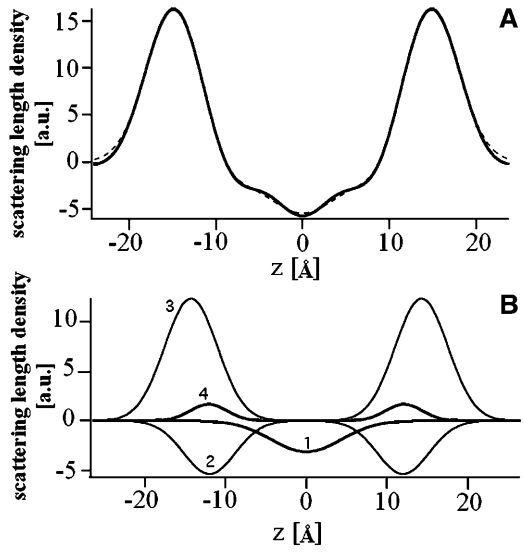

FIGURE 8 Neutron scattering length density profiles of lipid bilayers and the VP1 peptide. (*A*) Neutron scattering density profile generated by a transect of a POPC/POPS (10:1 molar ratio) membrane bilayer, taken perpendicular to the bilayer surface (*solid line*) in the presence of VP1 peptide. Each profile was determined at 8% ^2H_2O contrast. (*B*) The VP1 peptide corresponds to the Gaussian curve (*4*), which is in the presence of a lipid bilayer. The superimposed curves represent the different submolecular lipid groups: polar head (*3*); methyl group (*1*), and alkyl chains (*2*).

acyl chain that have a larger scattering length than the adjacent methylenes because of fewer hydrogens, which indicates that the lowest levels are produced by lipid terminal methyl groups, demarking the center of the bilayer hydrophobic core (King and White, 1986). The extra hydrogen on the terminal methyl group creates the central trough that corresponds to zero on the *x* axis. The scattering density profiles (Fig. 8 *A*) in the presence of the peptide are thought to be typical of protein penetration into an anionic POPC/POPS membrane (Dante et al., 2002; Hauβ et al., 2002; King and White, 1986).

To find a more quantitative description of the changes introduced by VP1 into the membrane structure, the experimental structure factors were fitted to a model membrane in reciprocal space. This was preformed using the reciprocal representation of Gaussian distributions as the fit function:

$$F(h) = scale * \sum_{i=1}^{n} \frac{area(i)}{width} * e^{-(2\pi * width * h)^2/2} * \cos(2\pi * position(i) * h), \quad (5)$$

where some constant factors are included in scale and the sum is taken over the number of Gaussian distributions used. The pure lipid bilayer from Fig. 7 *A* was partitioned into three Gaussian distributions corresponding to the methyl groups (*1*), alkyl chains (*2*), and polar headgroups, which also include the glycerol backbone (*3*). The parameters of the Gaussians were amplitude, position, and width. The width is a single parameter for all three Gaussians. This is a minimal model, obtained by parsing the lipid molecules in only three molecular groups to keep the number of parameters as low as possible. The model was fitted to the five structure factors of the lipid membrane keeping the area *A*, which is the calculated scattering length of the molecular groups, and the position of the methyl groups ($z = 0$) as fixed parameters. The positions of the headgroups and alkyl chains, and the width of the Gauss functions were therefore free parameters of the fit. To scale the absolute scattering length to the experimental data an appropriate scaling factor was used as the fourth fitting parameter. Fig. 7 *A* shows the experimental curve (*solid line*) and the fitted profile (*dotted line*) follow a similar trend. The fitted profile is decomposed into the individual Gaussian distributions in Fig. 7 *B*, and the final parameters are listed in Table 5. To obtain a good fit to the structure factors of the membrane sample with VP1 peptide, we had to introduce a fourth Gaussian distribution to account for the additional scattering length of the peptide. Fig. 8 *A* shows the experimental profile and the fitted profile for the sample, with VP1 peptide overlapping perfectly. Again the decomposed Gaussians are shown in Fig. 8 *B*. As seen in Table 5, beside the width of Gaussian 1, the three Gaussian curves representing the lipid molecules were kept unchanged with respect to the model already described. Here, the width of the methyl group and the area, width, and position of the fourth Gaussian were considered as free parameters. Comparison of Fig. 7 *B* and Fig. 8 *B* suggest that VP1 perturbs the alkyl chain region, where VP1 has an area of 5.4×10^{-13} cm^2 (Table 5) and is positioned at 12.5 Å.

TABLE 5 Parameters of the Gaussian fits in reciprocal space

	Area of the Gaussian (10^{-13} cm^2)	Position (Å)	Width (Å)
Gauss 1: methyl groups			
A	−9.6	0.0	3.7 ± 0.2
B	−9.6	0.0	4.6 ± 0.1
Gauss 2: alkyl chains			
A	−24.4	13.6 ± 0.5	3.7 ± 0.2
B	−24.4	13.6	3.7
Gauss 3: headgroups			
A	57.3	16.4 ± 0.1	3.7 ± 0.2
B	57.3	16.4	3.7
Gauss 4: VP1			
B	4.6	12.5 ± 0.05	2.9 ± 0.1

A, POPC/POPS membrane at 92:8 mol/mol; *B*, POPC/POPS membrane in the presence of VP1. Numbers without errors are fixed parameters. For *A* values, the width of Gaussian 1–3 is a single parameter.

This value is in very good agreement with the scattering length density of VP1 calculated from its chemical structure, and in a peptide/lipid ratio of 1:33, which is 6.04×10^{-13} cm^2. It should be noted that the width of the Gaussian curve for the methyl group in Fig. 8 *B* (6.4 Å) is larger than in Fig. 7 *B* (3.7 Å). This would suggest that the peptide perturbs the middle of the bilayer because the methyl region is enlarged. An attempt to fit the peptide sample with only three Gaussian distributions as in the case of the pure lipid sample failed. Even the liberation of the width in the methyl group distribution resulted in a bad fit. This is a strong indication that the additional scattering length of the peptide is really being measured in the neutron diffraction experiment.

Additional support for the penetration of the peptide into the lipid bilayer is given by the water distribution across the membrane (Fig. 9). Fig. 9 shows the water distribution profile

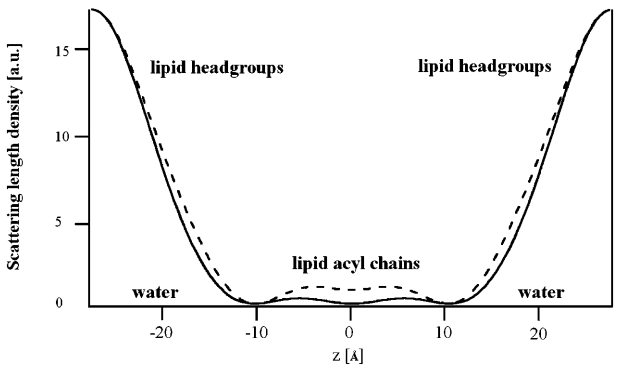

FIGURE 9 Distribution of the water in the unit cell showing the water distribution between 50% and 8% ^2H_2O for the pure lipid sample (*solid line*) and the peptide (*dotted line*). The distribution centered at ±27.5 Å shows a nearly Gaussian shaped intrabilayer distribution, which goes to nearly zero at the center of the bilayer (0 Å) for pure lipid. In the case of the peptide sample the distribution of water (deuterons) is increased in the center of the bilayer and in the deeper region of the alkyl chains. This increased distribution is due to the exchanged protons of the peptides or to water molecules attached to peptide. In addition, an enhanced scattering length is seen around ±15 Å, which is near the backbone region.

in stacks of POPC/POPS (*solid line*) and lipid-containing VP1 (*dotted line*). The intralamellar water (seen as scattering length density difference of 50% − 8% ^2H_2O) can be observed at the far corners of the plot. In the pure lipid sample a near flat distribution in the lipid core region is observed, whereas in the lipid/peptide sample (*dashed line*) some water has penetrated this region. In the pure lipid bilayers, the water density in the core is marginal; the enhanced concentration in the peptide sample presumably originates from the insertion of the VP1 peptide, which could facilitate water penetration deep into the bilayer.

DISCUSSION

It has previously been suggested that the in vivo activation of m-calpain, may involve interactions between the membrane and an oblique-orientated α-helix, located in domain V of the enzyme (Brandenburg et al., 2002; Daman et al., 2001). To investigate this suggestion, we have used a variety of biophysical techniques to study the membrane interactions of a peptide homolog of this segment (VP1) with lipid assemblies mimetic of naturally occurring membranes.

It has previously been shown that VP1 primarily adopts β-sheet structures in solution but is predominantly α-helical in the presence of pure anionic lipid SUVs (Brandenburg et al., 2002). Consistent with these results, this study showed VP1 (8 mM) to adopt α-helical structure (~45%) in the presence of DMPC/DMPS SUVs under a variety of conditions (Fig. 6, Tables 2 and 3). These levels of α-helicity were not significantly affected when the relative levels of total SUV lipid/VP1 were varied between 10:1 and 100:1 (Fig. 6). Moreover, these levels of VP1 α-helicity remained effectively constant when the anionic lipid content of SUVs was varied between 1% and 10% (Table 2 and Fig. 6 *A*). Similar levels of α-helicity were also shown by lower concentrations of VP1 in the presence of anionic lipid (Table 3), clearly eliminating peptide concentration effects and anionic lipid content as contributory to α-helix formation. When these results are taken with the observation that in 90% trifluoroethanol VP1 showed ~45% α-helicity (data not shown), it is suggested that VP1 may require the amphiphilic environment of the interface to adopt α-helical structure rather than a specific requirement for anionic lipid. Consistent with this suggestion, the surface activity of VP1 monolayers was studied and the molecular area occupied by the peptide in these monolayers at collapse pressure was determined as 164 Å^2 (Fig. 2), which is consistent with the presence of α-helical structure in VP1 (Fidelio et al., 1986).

The ability of VP1 to interact with a variety of lipid monolayers was investigated using an initial surface pressure of 30 mN m^{-1}, usually taken as representative of that of naturally occurring membranes. It was found that increasing levels of anionic lipid within DMPC/DMPS monolayers (between 1% and 10%), correlated strongly with the progressively greater ability of VP1 to insert into these

membranes (Figs. 4 and 5). Repeated experiments at a fixed pressure of 30 mNm^{-1} gave similar levels of insertion, implying that the hyperbolic curves observed in Figs. 4 *A* and 5 *A* do represent saturation of the system rather than pressure-induced inhibition of further insertion by the peptide. Although the monolayer may therefore support maximal α-helix formation by VP1, insertion by the peptide would appear to have a specific requirement for anionic lipid, possibly supporting the involvement of a snorkelling effect to accommodate the sole arginine residue of VP1.

Neutron diffraction studies were used to investigate the interactions of VP1 with bilayers formed from physiologically relevant lipids. It was found that the peptide was able to localize to the central core region of POPC/POPS (10:1 molar ratio) bilayers. Although our results do not directly demonstrate oblique-angled membrane penetration by the GTAMRILGGVI segment, they would be consistent with a mechanism of membrane penetration that involves anionic lipid and snorkelling by the segment's arginine residue, allowing the strongly hydrophobic C-terminal region of the GTAMRILGGVI α-helix (Fig. 10) to penetrate the membrane hydrophobic core. This is shown schematically in Fig. 11.

The effect of varying the fatty acid chains possessed by lipid monolayers on VP1/monolayer interactions was investigated. It was found that when the phosphatidylcholine/phosphatidylserine ratio of monolayers was maintained at 10:1, although VP1 showed similar final levels of interaction with all lipid monolayers studied, the peptide demonstrated kinetics that varied with the nature of the lipid acyl chain (Fig. 3). It can be seen from Fig. 3 that VP1 achieved maximal insertion into DMPC/DMPS monolayers five times faster than into DOPC/DOPS monolayers (300 s and 1500 s, respectively). The rank order of these rates of insertion correlates to that of the packing densities shown by the fatty

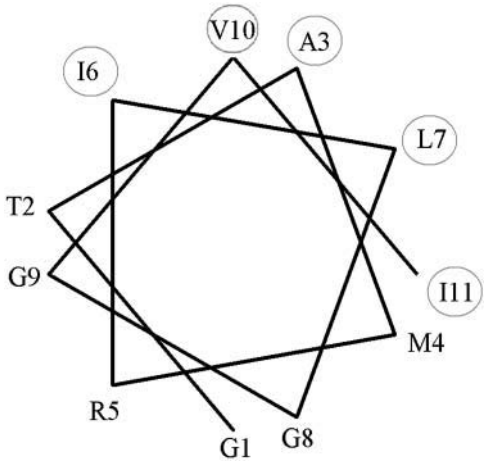

FIGURE 10 Two-dimensional axial projection of VP1 showing the primary structure of the GTAMRILGGVI segment from domain V of m-calpain represented as a two-dimensional axial projection. It can be seen that there is a localization of strongly hydrophobic leucine and isoleucine residues in the C-terminal region of the α-helix.

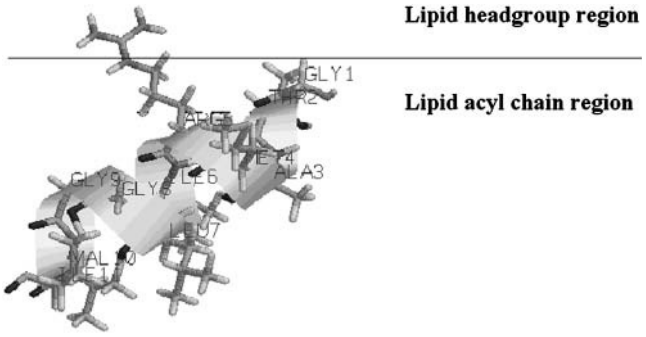

FIGURE 11 Putative model for the membrane interaction for VP1 peptide. Based on our results and those of previous authors, a schematic model has been constructed for the VP1 peptide (Brandenburg et al., 2002). We have arbitrarily shown the peptide inserted into the membrane at an angle of 45° relative to membrane surface. However, all known tilted peptides adopt an angle between 30° and 60°.

acid chains forming these monolayers. This would suggest that hydrophobic forces play a role in the lipid monolayer interactions of VP1 and thereby support the view that the peptide possesses an ability to penetrate the hydrophobic core of membranes, consistent with our neutron diffraction data.

In summary, our results clearly suggest that the m-calpain GTAMRILGGVI segment is able to form a membrane-interactive α-helix. Our results also suggest that the membrane interactions of this segment may involve penetration of the membrane hydrophobic core via a smorkelling mechanism that requires the presence of anionic lipid. The results suggest that domain V of m-calpain possesses the potential for lipid/membrane interaction and in Fig. 11 we propose a model based on the experimental results. There is clear evidence that such lipid interactions are able to trigger the cascade of events leading to autolysis and generation of the mature, active form of the enzyme (Goll et al., 2003). Currently, there is no known function for m-calpain domain V but it is known that upon activation, the major part of the domain is autolytically cleaved from the enzyme (Goll et al., 2003). We suggest that domain V may play a role in triggering the activation of m-calpain via lipid/membrane interactions before autolysis.

The authors thank Jörg Howe, Division of Biophysics, Forschunginstitut Borstel, Germany, for his assistance with FTIR analysis. We also thank Kia Balali-Mood, University of Edinburgh, for his technical assistance in the construction of the diagram representing VP1 peptide interacting with the membrane. Finally, we thank Giuliano Siligardi for confirming the structure of VP1 using CD analysis.

REFERENCES

Alminana, N., M. A. Alsina, M. Espina, and F. Reig. 2003. Synthesis and physicochemical study of the laminin active sequence: SIKVAV. *J. Colloid Interface Sci.* 263:432–440.

Ambroggio, E. E., F. Separovic, J. Bowie, and G. D. Fidelio. 2004. Surface behaviour and peptide-lipid interactions of the antibiotic peptides, Maculatin and Citropin. *Biochim. Biophys. Acta.* 1664:31–37.

Arthur, J. S., and C. Crawford. 1996. Investigation of the interaction of m-calpain with phospholipids: calpain-phospholipid interactions. *Biochim. Biophys. Acta.* 1293:201–206.

Branca, D. 2004. Calpain-related diseases. *Biochem. Biophys. Res. Commun.* 322:1098–1104.

Birdi, K. S. 1999. Self-Assembly Monolayer Structures of Lipids and Macromolecules at Interfaces. Kluwer Academic, Dordrecht, The Netherlands.

Bradshaw, J. P., R. J. Bushby, C. C. Giles, M. R. Saunders, and A. Saxena. 1997. The headgroup orientation of dimyristoylphosphatidylinositol-4-phosphate in mixed lipid bilayers: a neutron diffraction study. *Biochim. Biophys. Acta.* 1329:124–138.

Bradshaw, J. P., M. J. Darkes, T. A. Harroun, J. Katsaras, and R. M. Epand. 2000. Oblique membrane insertion of viral fusion peptide probed by neutron diffraction. *Biochemistry.* 39:6581–6585.

Bradshaw, J. P., S. M. Davies, and T. Hauβ. 1998. Interaction of substance P with phospholipid bilayers: a neutron diffraction study. *Biophys. J.* 75: 889–895.

Brandenburg, K., F. Harris, S. Dennison, U. Seydel, and D. Phoenix. 2002. Domain V of m-calpain shows the potential to form an oblique-orientated alpha-helix, which may modulate the enzyme's activity via interactions with anionic lipid. *Eur. J. Biochem.* 269:5414–5422.

Carafoli, E., and M. Molinari. 1998. Calpain: a protease in search of a function? *Biochem. Biophys. Res. Commun.* 247:193–203.

Chakrabarti, A. K., S. Dasgupta, R. H. Gadsden, E. L. Hogan, and N. L. Banik. 1996. Regulation of brain m calpain Ca2+ sensitivity by mixtures of membrane lipids: activation at intracellular Ca2+ level. *J. Neurosci. Res.* 44:374–380.

Crawford, C., N. R. Brown, and A. C. Willis. 1990. Investigation of the structural basis of the interaction of calpain II with phospholipid and with carbohydrate. *Biochem. J.* 265:575–579.

Daman, A., F. Harris, S. Biswas, J. Wallace, and D. A. Phoenix. 2001. A theoretical investigation into the lipid interactions of m-calpain. *Mol. Cell. Biochem.* 223:159–163.

Dante, S., T. Hauβ, and N. A. Dencher. 2002. Beta-amyloid 25 to 35 is intercalated in anionic and zwitterionic lipid membranes to different extents. *Biophys. J.* 83:2610–2616.

Duff, K. C., P. R. Gilchrist, A. M. Saxena, and J. P. Bradshaw. 1994. Neutron diffraction reveals the site of amantadine blockade in the influenza A M2 ion channel. *Virology.* 202:287–293.

Fidelio, G. D., B. M. Austen, D. Chapman, and J. A. Lucy. 1986. Properties of signal-sequence peptides at an air-water interface. *Biochem. J.* 238: 301–304.

Goll, D. E., V. F. Thompson. H. Li, W. Wei, and J. Cong. 2003. The calpain system. *Physiol. Rev.* 83:731–801.

Hauβ, T., S. Dante, N. A. Dencher, and T. H. Haines. 2002. Squalane is in the midplane of the lipid bilayer: implications for its function as a proton permeability barrier. *Biochim. Biophys. Acta.* 1556:149–154.

Hosfield, C. M., J. S. Elce, P. L. Davies, and Z. C. Jia. 1999. Crystal structure of calpain reveals the structural basis for Ca2+-dependent protease activity and a novel mode of enzyme activation. *EMBO J.* 18: 6880–6889.

Hosfield, C. M., J. S. Elce, and Z. Jia. 2004. Activation of calpain by Ca2+: roles of the large subunit N-terminal and domain III–IV linker peptides. *J. Mol. Biol.* 343:1049–1053.

Huang, Y., and K. K. Wang. 2001. The calpain family and human disease. *Trends Mol. Med.* 7:355–362.

Imajoh, S., H. Kawasaki, and K. Suzuki. 1986. The amino-terminal hydrophobic region of the small subunit of calcium-activated neutral protease (Canp) is essential for its activation by phosphatidylinositol. *J. Biochem. (Tokyo).* 99:1281–1284.

Johnson, G. V., and R. P. Guttmann. 1997. Calpains: intact and active? *Bioessays.* 19:1011–1018.

Keller, R. C., J. A. Killian, and B. Kruijff. 1992. Anionic phospholipids are essential for alpha-helix formation of the signal peptide of prePhoE upon interaction with phospholipid vesicles. *Biochemistry.* 31:1672–1677.

King, G., and S. White. 1986. Determining bilayer hydrocarbon thickness from neutron diffraction measurements using strip-function models. *Biophys. J.* 49:1047–1054.

Melloni, E., and S. Pontremoli. 1989. The calpains. *Trends Neurosci.* 12: 438–444.

Ono, Y., H. Sorimachi, and K. Suzuki. 1998. Structure and physiology of calpain, an enigmatic protease. *Biochem. Biophys. Res. Commun.* 245: 289–294.

Perrin, B. J., and A. Huttenlocher. 2002. Calpain. *Int. J. Biochem. Cell Biol.* 34:722–725.

Reverter, D., S. Strobl, C. Fernandez-Catalan, H. Sorimachi, K. Suzuki, and W. Bode. 2001. Structural basis for possible calcium-induced activation mechanisms of calpains. *Biol. Chem.* 382:753–766.

Rizo, J., and T. C. Sudhof. 1998. C-2-domains, structure and function of a universal Ca2+-binding domain. *Biol. Chem.* 273:15879–15882.

Saido, T. C., M. Shibata, T. Takenawa, H. Murofushi, and K. Suzuki. 1992. Positive regulation of mu-calpain action by polyphosphoinositides. *Biol. Chem.* 267:24585–24590.

Sato, K., and S. Kawashima. 2001. Calpain function in the modulation of signal transduction molecules. *Biol. Chem.* 382:743–751.

Sorimachi, H., and K. Suzuki. 2001. The structure of calpain. *J. Biochem. (Tokyo).* 129:653–664.

Sospedra, P., I. Haro, M. A. Alsina, F. Reig, and C. Mestres. 1999. Physicochemical interaction of a lipophilic derivative of HAV antigen VP3 (110–121) with lipid monolayers. *Mater. Sci. Eng. C.* 8–9:543–549.

Strobl, S., C. Fernandez-Catalan, M. Braun, R. Huber, H. Masumoto, K. Nakagawa, A. Irie, H. Sorimachi, G. Bourenkow, H. Bartunik, K. Suzuki, and W. Bode. 2000. The crystal structure of calcium-free human m-calpain suggests an electrostatic switch mechanism for activation by calcium. *Proc. Natl. Acad. Sci. USA.* 97:588–592.

Tompa, M. 2001. Identifying functional elements by comparative DNA sequence analysis. *Genome Res.* 11:1143–1144.

Verdaguer, N., S. Corbalan-Garcia, W. F. Ochoa, I. Fita, and J. C. Gomez-Fernandez. 1999. Ca2+ bridges the C2 membrane-binding domain of protein kinase C alpha directly to phosphatidylserine. *EMBO J.* 18:6329–6338.